metals

MDPI

Article

Tribological Properties of SPS Reactive Sintered Al/MoS_2 Composites

Marek Kostecki *, Krzysztof Kulikowski, Dorota Moszczyńska and Andrzej Roman Olszyna

Faculty of Materials Science and Engineering, Warsaw University of Technology, Woloska St. 141, 02-507 Warsaw, Poland; krzysztof.kulikowski@pw.edu.pl (K.K.); dorota.moszczynska@pw.edu.pl (D.M.); andrzej.olszyna@pw.edu.pl (A.R.O.)

* Correspondence: marek.kostecki@pw.edu.pl

Abstract: In search of opportunities to improve mechanical properties and abrasion resistance, composites based on aluminum reinforced with MoS_2 particles were produced. The authors' previous research indicated the possibility of obtaining hard dispersion precipitates of the $Al_{12}Mo$ intermetallic phase as a result of the reaction of the composite components at a temperature exceeding 550 °C during the SPS (Spark Plasma Sintering) process. This work focused on optimizing the SPS consolidation process and assessing the microstructure and mechanical properties of the obtained materials. A series of experiments proved that by increasing the amount of the strengthening phase and increasing the process temperature, a significant amount of $Al_{12}Mo$ and Al_5Mo strengthening phases is produced. Exceptionally good dispersion of reinforcing particles and the presence of layered MoS_2 crystals, while ensuring optimal parameters of the synthesis process, lead to a change in friction mechanisms and improved abrasion resistance through an approximately 30-fold decrease in the wear factor.

Keywords: aluminum; composites; molybdenum disulfide; spark plasma sintering; tribological properties

check for updates

Citation: Kostecki, M.; Kulikowski, K.; Moszczyńska, D.; Olszyna, A.R. Tribological Properties of SPS Reactive Sintered Al/MoS_2 Composites. *Metals* **2024**, *14*, 1326. https://doi.org/10.3390/met14121326

Academic Editors: Wenming Jiang and Abdollah Saboori

Received: 13 October 2024
Revised: 14 November 2024
Accepted: 20 November 2024
Published: 24 November 2024

Copyright: © 2024 by the authors. Licensee MDPI, Basel, Switzerland. This article is an open access article distributed under the terms and conditions of the Creative Commons Attribution (CC BY) license (https://creativecommons.org/licenses/by/4.0/).

1. Introduction

Metallic matrix composites have become the most desirable construction materials in recent decades, replacing classic, light alloys in many applications. Due to their specific properties (increased fatigue resistance, hardness, abrasion resistance, and reduced thermal expansion coefficient), they are widely used in the aviation, automotive, and space industries [1–3]. Although their processing and recycling may pose some difficulties, the advantages resulting from use still encourage involvement in their further development. An undoubted advantage that makes aluminum-based composites superior to multi-phase alloys is the concept of introducing virtually any phases and designing their spatial arrangement. The possibility of using lower volume fractions of the nanometer-sized reinforcing phase will also be important [4,5]. Unconventional synthesis methods, including mechanical alloying or the use of incremental shaping techniques—3D printing have become very helpful in implementing these tasks [6].

In order to give the material additional features, ceramic materials are an important component of these composites. Classic examples concern the use of SiC, Al_2O_3, or ZrO_2, which influence hardness, tribological properties, and the possibility of increasing the operating temperature [7]. The mentioned reinforcement may be in the form of both particles and fibers. Fibers, including carbon fibers, seem to be perfect for reinforcing metal-matrix composites, but due to the reactions between the reinforcement and the matrix occurring at the interface and problems with wetting, their production is technically difficult. Similar problems also apply to the dispersed phase in partial composites, where ex situ methods, apart from the previously mentioned poor wetting by the matrix, promote agglomeration, lack of homogeneity, and the introduction of additional impurities.

An alternative way to bypass some of the mentioned limitations and ensure the thermodynamic stability of the material is to deliberately induce a chemical reaction between the components of the composite and strengthen the alloy with in situ precipitates. In situ synthesizing can be obtained by many approaches, such as reactive hot pressing, combustion synthesis, friction stir processing, or direct melt oxidation [8]. This composite synthesis has been widely followed by researchers because of several advantages over conventional casting, such as fine particle size, clean interface, good wettability of the reinforcement with the matrix, and homogeneous distribution of the reinforcement. Commonly used reinforcements for aluminum and its alloys that can be produced in situ are Al_2O_3, AlN, TiB_2, TiC, ZrB_2, and Mg_2Si [9].

Lubrication is of key importance in aluminum-based composites manufactured to ensure increased tribological properties. Ensuring lubrication at the contacts of interacting components is always a demanding task, especially in extreme conditions such as vacuum. In systems where conditions prevent liquid lubrication, solid lubricants such as graphite and molybdenum disulfide are most often used. Research on the use of molybdenum disulfide as a solid lubricant has been conducted since the 1970s [10]. Unlike graphite, MoS_2 does not require moisture for proper crystal delamination, which allows it to be used in dry gas and vacuum environments, also allowing its use in the space industry [11]. When working in a moisture-free environment, the wear mechanism of molybdenum disulfide changes. The delaminated fragments of MoS_2 crystals adhere to the substrate, creating a film separating the two mating friction surfaces, which wear out over time by detaching small flakes from it. In the presence of moisture in the working environment, the removed MoS_2 layers do not adhere to the surface and agglomerate, which leads to an increase in the friction coefficient.

There are few literature references to composites strengthened only with MoS_2 crystals, although they concern both metallic matrixes such as Cu, Fe, Al [12–16] and polymeric materials [17,18]. These works focus primarily on tribological effects. The addition of MoS_2 is much more often used in hybrid composites as the second phase, primarily aimed at reducing the friction coefficient, which in the vast majority of cases brings very positive results. The presence of MoS_2 simultaneously leads to a lower friction coefficient, reduces wear, and sometimes leads to a reduction in the grain size of the matrix material [19–26]. Unfortunately, there is also a slight reduction in the hardness and strength of such composites, especially when the MoS_2 content exceeds 10% by volume [13]. However, the positive effects of adding a solid lubricant to the composite may depend on many other factors that were not taken into account in the previously mentioned works. The most important of them is the possibility of reactions occurring at the stage of the production process. The second important factor may be the form in which the MoS_2 particles are used, namely whether they are bulk crystals or nanoparticles, e.g., with a 2D flake morphology.

In the case of composites based on CuSn alloy [12], despite the decrease in the friction coefficient, the wear rate of composites containing MoS_2 (0–40% by volume) increases significantly with the amount of MoS_2 added. This behavior was related to the formation of brittle $CuMo_2S_3$ phase in composites. In this case, MoS_2 was ineffective as a solid lubricant due to its instability and reactivity with the metal at the sintering temperature.

Research carried out a few years later on pure copper with the addition of up to 40% MoS_2 [13] confirmed the formation of the $CuMo_2S_3$ phase only when the content of solid lubricant exceeded 20%. At the same time, despite the reduction in the friction coefficient, there was significantly accelerated wear and a reduction in strength, confirmed in a bending test, regardless of the amount of the additive.

A similar situation occurs when the matrix is iron [14]. The tests showed that for a pure iron matrix, the reaction of MoS_2 with the matrix took place already at a temperature of 850 °C, i.e., lower than expected based on the Gibbs energy calculation. The reaction product was iron sulfides or mixed iron and molybdenum sulfides. Additions of alloying elements, such as phosphorus or molybdenum, delayed the reaction of MoS_2 with iron.

The composite itself performed worse in tribological tests than the composite that did not react with the lubricant particles.

The research initiated by the authors of this article was aimed at obtaining a new composite based on an aluminum alloy with the addition of MoS_2 nanoflakes [27,28]. It confirmed a very similar phenomenon of the formation of a new phase to the one described earlier. During the synthesis process using the SPS method, the reaction of the components led to the in situ formation of the $Al_{12}Mo$ intermetallic phase and a significant change in the mechanical properties.

Research related to the formation of the dispersive $Al_{12}Mo$ phase was later confirmed in more detail by Fan and coworkers [29]. The authors tested composites based on pure aluminum with the addition of 0.5 to 1.5% MoS_2 and showed that it can react to form Al_2S_3 and $Al_{12}Mo$ at a temperature of 630 °C. The interfacial reaction generates a strong chemical bond between the matrix and the reinforcement. In situ formed $Al_{12}Mo$ plays an important role in improving the mechanical properties by grain refinement, blocking dislocation movement, and load transfer. Load transfer is the dominant mechanism responsible for the improvement in strength based on the calculation of the contribution of each mechanism. Aluminum composites, with the addition of 1.5% MoS_2 by weight, showed the highest tensile of 234 MPa and yield strength of 210 MPa, which is an improvement over unreinforced Al (UTS of 145 MPa and YS of 110 MPa) while maintaining a fairly high ductility of 17% elongation.

In the present research, the authors decided to investigate how the observed strengthening phenomenon in the presence of excess MoS_2 particles will affect the tribological properties. Therefore, it was decided to increase the proportion of MoS_2 by 10% in volume. The synthesis was carried out under conditions that ensured the formation of dispersive precipitates of the $Al_{12}Mo$ intermetallic phase. The time and temperature variables for the composite synthesis proposed in the experiment were intended to check the kinetics of precipitate formation.

2. Materials and Methods

Aluminum and MoS_2 powders were used to obtain composites that were 99.9% pure. The manufacturer of the aluminum compound, Atlantic Equipment Engineers (Upper Saddle River, NJ, USA), reported an average powder size of 325 mesh. The larger particles are characterized by a slightly elongated shape, while the finer fraction has a shape close to spherical. Single, large particles with an average equivalent diameter exceeding 17 µm can be observed. The average elongation parameter for the Al powder particles is 1.60, which indicates a deviation from the spherical shape. MoS_2 was obtained from Nanostructured and Amorphous Materials, Inc. (NanoAmor, Los Alamos, NM, USA) and has a flake morphology, an average transverse dimension of 680 nm, and a thickness ranging from 20 to 40 nm.

The compositions of the starting powder mixtures and the SPS process conditions were selected based on the phase diagram of the Al-MoS_2 system. The proposed volume fractions of MoS_2 in the composite precursors were 10% and 5%. After weighing the appropriate amount of each powder, they were prepared for homogenization in a horizontal ball mill (Gabbrielli Technology, Calenzano, Italy). Milling was carried out for 8 h at a speed of 300 rpm in the presence of isopropyl alcohol and Al_2O_3 balls with a diameter of d = 2 mm in a weight ratio of 3:1. The mill rotational speed used was selected to introduce as few defects as possible into the layered crystals and to avoid deformation and hardening of the aluminum powder particles. Previous research has shown that defoliation may result in the formation of much thinner MoS_2 flakes during milling. In the next step, the suspensions were dried and granulated on sieves with a mesh diameter of 0.3 mm. Example photos of the starting MoS_2 powder and the powder mixture are shown in Figure 1. After the mixing process, the Al powder grains were quite evenly stuck with MoS_2 flakes, which did not prevent the mixture from forming local agglomerates of molybdenum sulfide. In the case

of the mixture with the addition of 5%, the presence of agglomerates of MoS_2 nanoparticles was also observed.

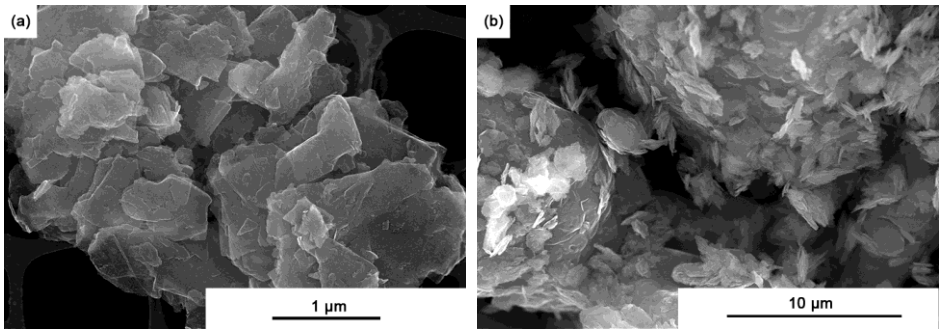

Figure 1. Powder morphologies of (**a**) MoS_2 and (**b**) Al+ MoS_2 10% vol. mixture.

The powder was sintered in an SPS device (HPD 10, FCT Systeme GmbH, Rauenstein, Germany) in an argon atmosphere in a graphite matrix with a diameter of φ = 20 mm at a pressure of p = 50 MPa. Each time, 8 g of the powder was weighed into the matrix. Maximum pressures were applied only from the moment the target temperature was reached, which was intended to enable the free removal of gases generated during the temperature increase. As a consequence, this allowed for reducing the number of closed pores and obtaining a denser composite. A minimum temperature of 550 °C and a sintering time of t = 4 min were selected based on the results of previously conducted research [27,30]. Ultimately, it was proposed to extend the sintering time by two and four times in order to assess the impact of time on the properties of the obtained composites and the amount of intermetallic phase formed. A summary of all the process parameters is presented in Table 1. A minimum of three samples were performed for each set of parameters, and all results presented represent the average value tested for these samples.

Table 1. Sintering parameters of composites Al/MoS_2.

Material	Sintering Time [min]			Sintering Presure [MPa]	Sintering Temperature [°C]
Al + MoS_2 10% vol.	4	8	16	50	550
	4	8	16		600
	4	8	16		650
Al + MoS_2 5% vol.	4	8	16	50	600
	4	8	-		650

The apparent density and porosity were calculated based on measurements using the hydrostatic method. Observations and photos of the microstructure of previously prepared metallographic sections were made using a metallographic microscope NIKON Eclipse MA200 metallographic microscope (NIKON, Tokyo, Japan) coupled with the program for stereological calculations, NIS-Elements. Detailed observations of the microstructure and analysis of the chemical composition were performed using two different types of scanning/transmission microscopes, Hitachi S3500N and Hitachi S5500N SEM (Hitachi, Manchester, UK) equipped with an energy-dispersive X-ray spectrometer (EDS) (Thermo Fisher Scientific, Waltham, MA, USA). The phase compositions of the tested samples were determined using a Bruker D8 Discover X-ray diffractometer (BRUKER, Billerica, MA, USA). A fully automated MMT X7B hardness tester coupled with a microscope (Matsuzawa Co., Ltd., Kawabe, Japan) was used for the hardness tests. Measurements were carried out on the entire surface of the samples in ten randomly selected places with a pressure of 19.61 N.

Frictional wear resistance tests were carried out using the "ball-on-disc" method, using the T-21 tribotester (ITEE, Radom, Poland), in accordance with the requirements specified

in the ASTM G 99-05 standard. The measurements were carried out at ambient temperature (22 ± 2 °C), without the use of external lubricants. Ceramic Al_2O_3 balls with a diameter of 6.35 mm and a polished surface (class G28) were used for testing. The measurements were carried out under a load of 2N, with a radius of 5 mm and a linear sliding speed of 0.1 m/s. For each sample, measurements were made at 1000 revolutions, which corresponds to a friction distance of the counter-sample of 31.42 m. Before testing, the surfaces of the sample and counter-sample were cleaned with acetone.

The wear resistance was determined based on measurements of the groove (wear) profile. The geometry of the furrow was determined using an optical profilometer (SENSOFAR, Terrassa, Spain), and on this basis, the volume of material used during the test was determined. The volumetric consumption rate was determined according to Equation (1):

$$W_v = \frac{V}{Fn \cdot s}\left[\frac{mm^3}{N \cdot m}\right] \quad (1)$$

where: V is the volume of used material calculated on the basis of the average cross-sectional area of the furrow, Fn—normal force, s—friction path.

3. Results and Discussion

3.1. Phase Composition and Microstructure

The prediction of the behavior of the mixture of compounds under the planned synthesis conditions was based on both the experiment and phase diagram. According to the data collected by Saunders [31], the solubility of Mo in Al in the solid state is limited. Al solid solution is stable up to 660 °C, where it decomposes in the peritectic reaction Al↔L+$Al_{12}Mo$. $Al_{12}Mo$ has a cubic structure and is stable up to 712 °C, where it decomposes as a result of the peritectic reaction $Al_{12}Mo \leftrightarrow L + Al_5Mo$. For the hexagonal Al_5Mo compound, there are three different crystallographic structures, which differ in the arrangement of the layers along the c-axis.

A good understanding of the reactions that occur between Al and MoS_2 was provided by a group of scientists from China who conducted calorimetric and thermogravimetric (DSC/TG) tests on a mixture of Al powder with 10 wt.%. MoS_2 [32]. At a temperature of 561 °C, an exothermic peak appeared on the DSC curve, which showed that the reaction between the components took place in the solid state at a temperature much lower than the melting point of Al. A further increase in temperature resulted in the appearance of another peak, this time endothermic, at a temperature of approximately 669 °C, which was associated with the melting of aluminum. Analysis of the diffractograms showed that during annealing at 630 °C, aluminum sulfide (Al_2S_3), Mo, and Mo-rich phases (Al_5Mo and $Al_{12}Mo$) were formed, and MoS_2 and aluminum did not react completely. When the sample was annealed at 680 °C, just above the melting point of Al, the reaction intensity increased, and the powders completely reacted. According to the DSC and XRD results, the reaction between MoS_2 and Al began at a temperature of 561 °C. During the reaction, MoS_2 first reacted with Al to give the products Mo and Al_2S_3. Al then reacted with Mo to form a series of Al_xMo_y compounds, the composition of which changed from Al-rich to Mo-rich phases with increasing temperature.

In the experiment, synthesis temperatures from 550 °C to 650 °C were proposed, while the time was initially selected as 4 min and extended twice and four times (to 8 and 16 min) until a plateau was reached in the sintering curve. The displacement of the matrix punches was then not recorded, which is a clear signal that there was no compaction progress. Diffusion of ingredients inside the material may still occur; however, the volume is relatively constant. Maintaining the longest process time at 650 °C was impossible for the Al+5%MoS_2 preparation because the material flowed out of the matrix. These preparations were, therefore, not subjected to further testing. The specificity of the SPS process, especially when a conductive material is synthesized, allows for a local temperature increase significantly above the assumed average values. The melting point of aluminum is 660.3 °C, so overheating to create a liquid phase is very possible with a limit of 650 °C.

There is also a high probability of such a temperature increase occurring locally; therefore, any process carried out at 650 °C could have involved the liquid phase.

Images taken in the BSE (backscattered electrons) mode clearly show differences in the chemical composition of the visible structures. Figures 2 and 3 show the microstructures of the obtained sinters. Areas rich in molybdenum will, therefore, be the lightest and those rich in aluminum the darkest. It can be assumed that, in the presented structures, dark gray aluminum grains are surrounded by unreacted MoS_2 (Figure 2a,b), and where the reaction has occurred, light precipitates containing molybdenum appear inside the aluminum grains (Figure 3a,b). EDS (energy-dispersive X-ray spectroscopy) analyses performed during the observations and the phase composition analyses presented below (Figure 4) confirm this description of the microstructure. A more detailed description of the phases, also taking into account electron diffraction, was presented in the authors' previous publication [28].

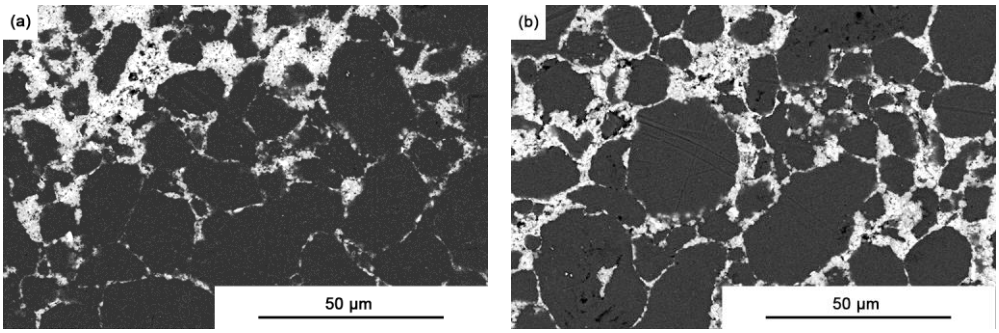

Figure 2. Microstructure of Al+ 5% vol. MoS_2 sinters obtained at (**a**) 600 °C and (**b**) 650 °C (sintering time 4 min.).

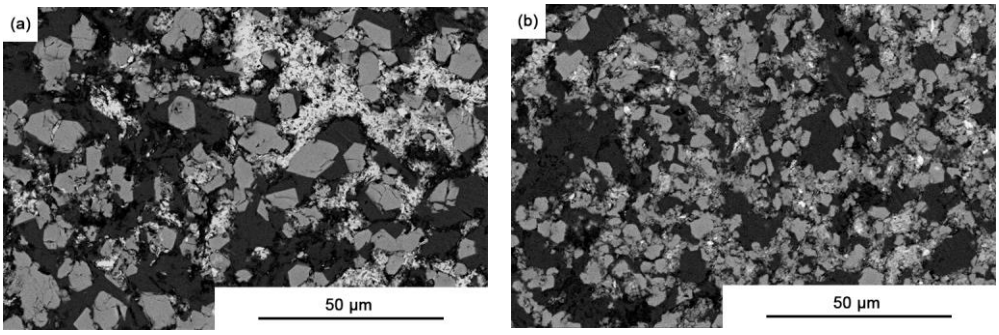

Figure 3. Microstructure of Al+ 10% vol. MoS_2 sinters obtained at (**a**) 600 °C and (**b**) 650 °C (sintering time 16 min.).

XRD tests showed the presence of $Al_{12}Mo$ and Al_5Mo phases in the sinters, but did not reveal the presence of Al_2S_3. Aluminum sulfide produced as a result of the synthesis can easily hydrolyze upon contact with water, producing hydrogen sulfide [33]. The water required for this reaction during sintering could originate from the residual moisture adsorbed on the particles of the powder mixture or from technical argon filling the sintering chamber. Evidence of such a reaction may be the intense smell of hydrogen sulfide accompanying "freshly" prepared specimens and during their contact with water after preparation. Therefore, it is possible that the Al_2S_3 produced in the SPS processes underwent hydrolysis, and small residues were not detected in the XRD examination.

Sintering carried out for the shortest time (4 min) and at the lowest temperature of 550 °C with 5% MoS_2 does not lead to the formation of intermetallic phases that can be observed microscopically. The examined microstructures of sinters presented in Figure 3 indicate that only from a temperature of 600 °C, we observe the reaction products of the composite components mainly in agglomerated areas, where very fine particles of aluminum powder are also present. Only a temperature of 650 °C ensures the presence

of fine crystalline precipitates at the boundaries of all powder particles surrounded by MoS_2 crystals. Regardless of the volume fraction, extending the sintering process time to 8 and 16 min leads to intensified growth of intermetallic phase crystals. Increasing the time activates both the process of thermal decomposition of MoS_2 and the diffusion of elements in the matrix material. The process carried out at a higher temperature also accelerates the nucleation process, and the microstructure is characterized by a much finer grain (Figure 3b).

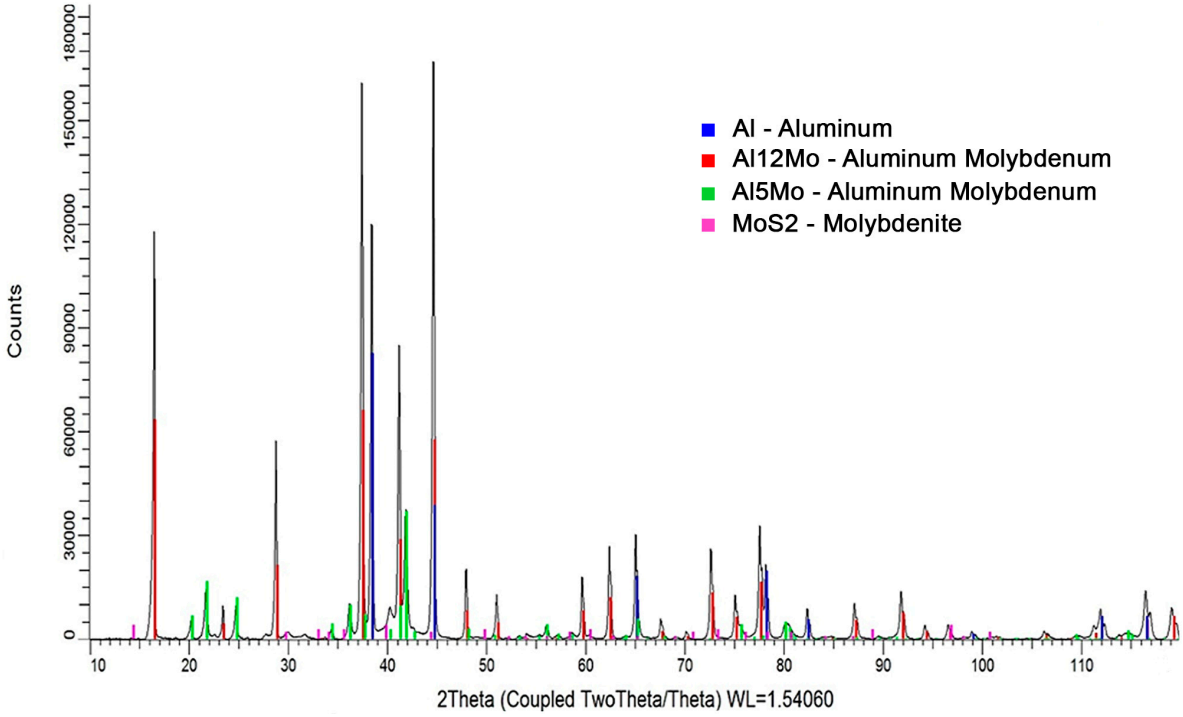

Figure 4. Diffraction pattern of the Al + 10% vol. MoS_2. sample sintered at 650 °C (10 min.).

Extending the sintering time to 16 min for both composites with the addition of 5% and 10% MoS_2 still does not lead to a complete reaction of the additive. The remains of MoS_2 flakes (Figure 5) are necessary for lubrication in the friction process; therefore, it is expected that providing a larger share of them in the composite will lead to an improvement in tribological properties. According to previous research, min. 2% of MoS_2 addition reduces the friction coefficient [27]. The flakes arranged themselves statistically in an unoriented way. Despite the axial compression, the crystals did not adopt a specific direction relative to the pressing axis.

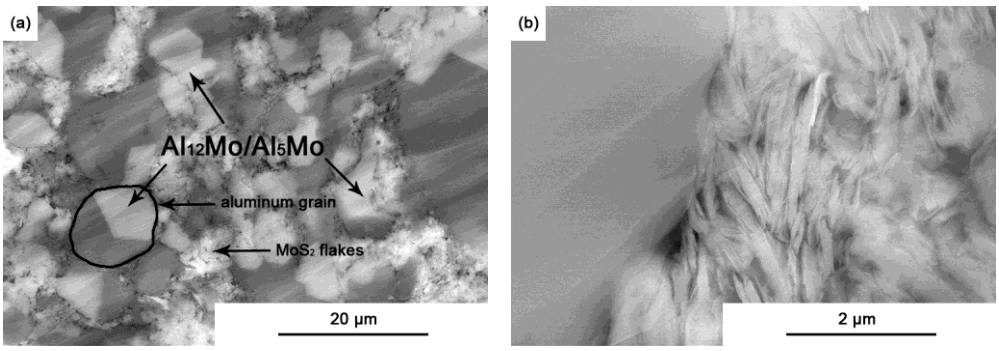

Figure 5. Microstructure of Al+ 10% vol. MoS_2 sinter (650 °C/16 min): (**a**) precipitation of the intermetallic phase inside Al grains and (**b**) MoS_2 flakes on the boundary of the powder particles.

3.2. Density and Hardness

The observed microstructure correlates perfectly with the results of the density and porosity tests. The graph below (Figure 6) presents the results of the apparent density of the produced composites. The theoretical densities of the powder mixtures are 2.832 g/cm^3 for the addition of 10% MoS_2 by volume and 2.764 g/cm^3 for 5% vol. MoS_2. Calculating the relative density was not possible due to the lack of precise data on the number and type of all phases formed in the composite as a result of the reaction between its components. Comparing the apparent density for individual compositions, it can be seen that with the addition of 5% MoS_2, lower density values were obtained, which is related to the lower share of the $Al_{12}Mo$ phase, for which the density is 3.12 g/cm^3 [34]. The highest apparent density is represented by sinters containing 10% MoS_2 obtained at a temperature of 650 °C and is 2.85 g/cm^3, which is higher than the theoretical density of the powder components. Although at a sintering temperature of 650 °C, the difference in apparent density is imperceptible, extending the sintering time from 8 to 16 min affects the open porosity (Figure 7). A longer sintering time makes it possible to close the open pores left in the structure by gaseous transformation products, such as H_2S.

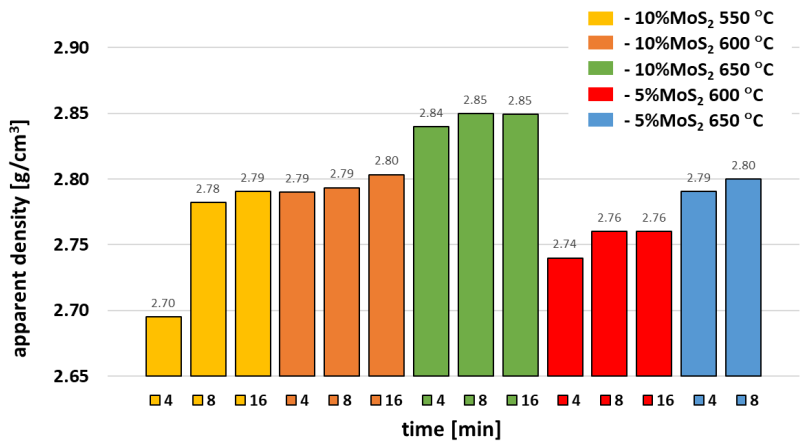

Figure 6. Apparent density of the Al/MoS_2 sinters.

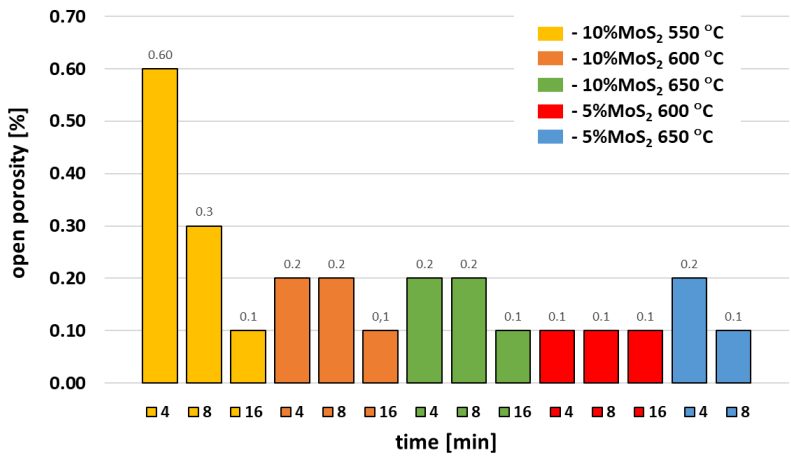

Figure 7. Open porosity of Al/MoS_2 sinters.

The hardness of composite sinters increases with increasing temperature and the extension of the sintering time (Figure 8). This is related to the synergistic effect of two factors: improved density and the appearance of hard in situ precipitates of intermetallic phases in the structure. However, it seems that the key parameter of the synthesis process influencing the hardness while providing adequate time for the reaction is the process temperature. Figure 8 shows the dependence of the hardness on the process temperature for the longest

sintering time of 16 min. While at a constant temperature, extending the time from 8 to 16 min resulted in an increase in hardness by a maximum of about 32%; the increase in temperature from 600 °C to 650 °C (within 16 min process) caused the hardness of the sinter to increase more than twice, from 84HV to 176.3 HV. The effect is even more visible for the Al + 5% vol. MoS_2, where the increase is more than tripled from 48HV to 152HV compared to the 8 min process at 650 °C. The analysis of density changes and growth kinetics of the intermetallic phase indicates that 10% molybdenum sulfide flakes generate some porosity related to the presence of unreacted MoS_2. The amount of the intermetallic phase produced at a temperature of 650 °C is slightly higher for the Al + 10% vol. MoS_2 composite (approx. 14%, which was confirmed by stereological calculation based on SEM BSE images); however, increasing the temperature does not linearly increase the proportion of in situ precipitates in the sinters. An additional factor influencing the increase in hardness is the refinement of the microstructure observed at the highest process temperature (Figure 3a,b).

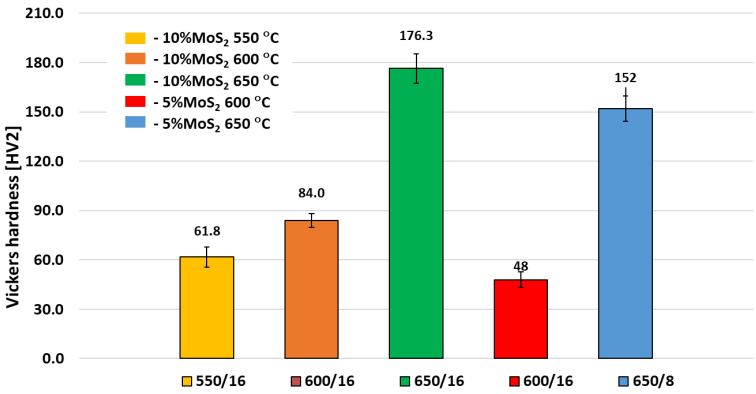

Figure 8. Vickers hardness HV2 of Al/MoS_2 sinters.

3.3. Tribological Behavior

Tribological tests were performed only for composites characterized by the highest hardness and thus the longest sintering time for each composition and temperature. In order to indicate the influence of the intermetallic phase generated during sintering, tests of the friction coefficient and wear rate were determined. Figure 9 shows the progression of the friction coefficient changes during the "ball-on-disk" testing, while Figure 10 presents the average values of the friction coefficients in the range of established friction (between 200 and 1000 rotations of the sample).

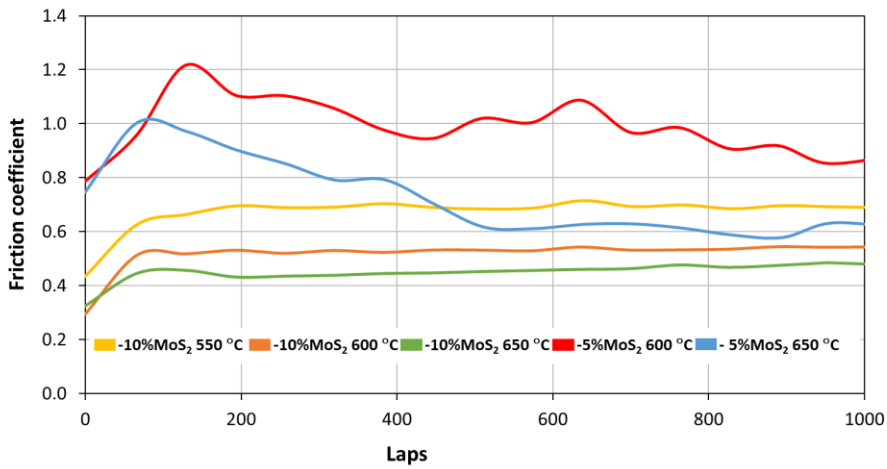

Figure 9. The course of changes in the friction coefficient during the wear resistance test of Al/MoS_2 composites.

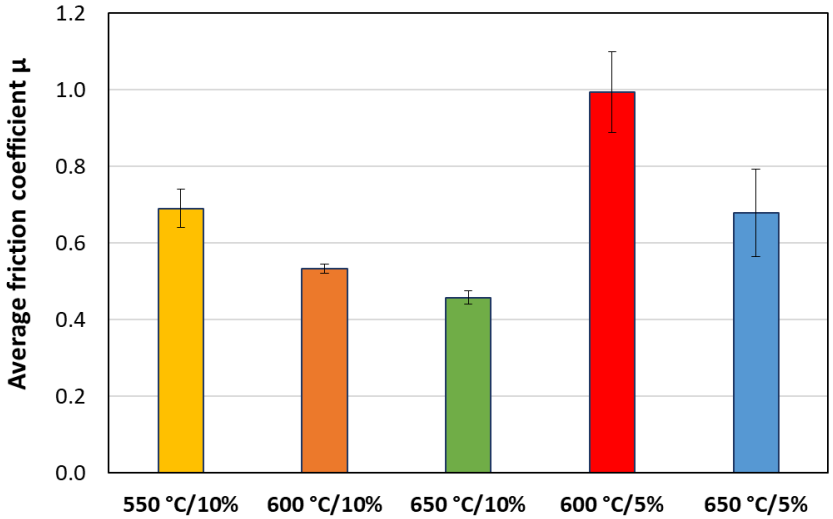

Figure 10. Average friction coefficient in the steady-state friction (range 200–1000 revolutions) of Al/MoS_2 composites.

In the initial phase of friction, an increase in the friction coefficients is observed, which is attributed to the run-in process of the friction pair. Due to the initial point contact geometry of the ball-plane interface and the associated high stresses in the contact area of the two friction bodies, rapid initial wear formation occurs. After approximately 100 rotations for samples containing 10% MoS_2, stabilization of the friction coefficient is observed (Figure 9). As the sintering temperature increases, the average value of the friction coefficient in the established friction range (between 200 and 1000 rotations) decreases from about 0.69 for the material sintered at 550 °C to approximately 0.53 for that sintered at 600 °C and down to about 0.46 for the material sintered at 650 °C (Figure 10).

The changes in the friction coefficient with respect to the sintering temperature are related to the variation in the density of the sintered materials (Figure 6) and their hardness (Figure 8). In the case of the sample sintered at 550 °C, significant plastic deformation of the substrate occurs during friction (Figure 11). This considerably limits the effect of the MoS_2 additive on the friction coefficient. During plastic deformation, fragments of the substrate move to a limited extent relative to one another, and the addition of 10% MoS_2 does not ensure their separation nor does it reduce the friction coefficient along the low-binding-energy planes. The increase in substrate hardness achieved through sintering at higher temperatures (600 °C and 650 °C) leads to a change in the wear characteristics, limiting the effects of plastic deformation in favor of abrasive wear. Consequently, the harder particles generated during friction move along with the counter-sample and are removed from the scratch area (Figures 12 and 13). The pressure of the ball on the substrate exceeds the strength of the interplanar bond in the MoS_2 structure, leading to shearing at stresses lower than those required for plastic deformation and decohesion of the substrate. The worn surface shows a granular character, and the scratch is shallow, but shows traces of cracks in the transfer layer (Figure 13). For the composite obtained at 650 °C, traces of chipping appear locally inside the scratch (Figure 13c), related to the removal of hard particles of intermetallic phases. This effect is caused by the presence of agglomerates of unreacted molybdenum sulfide, limiting the cohesion of the sinter. The surface microstructures after the tests are shown in Figures 11–13.

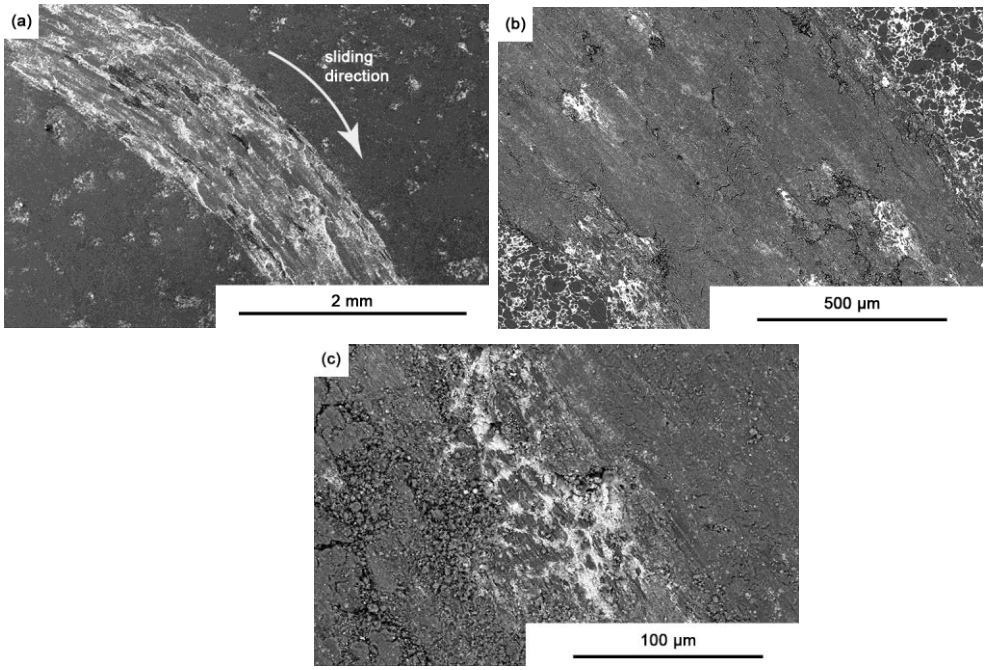

Figure 11. SEM micrographs of worn surfaces of Al-10% vol. MoS_2 composite sintered at 550 °C; (**a**–**c**) show different magnification of the same spot.

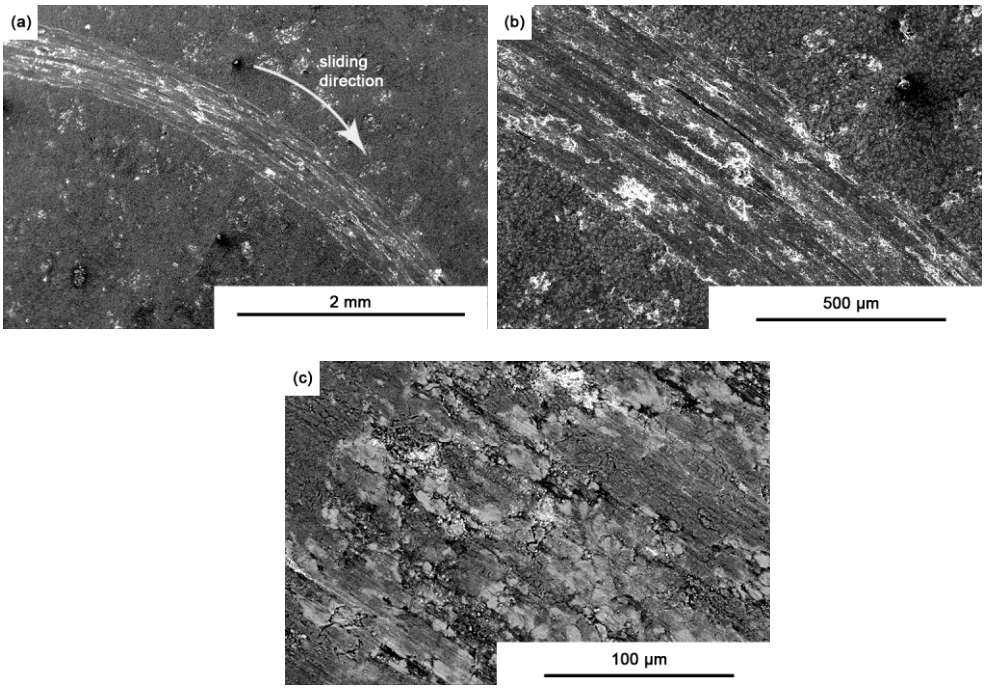

Figure 12. SEM micrographs of worn surfaces of Al-10% vol. MoS_2 composite sintered at 600 °C; (**a**–**c**) show different magnification of the same spot.

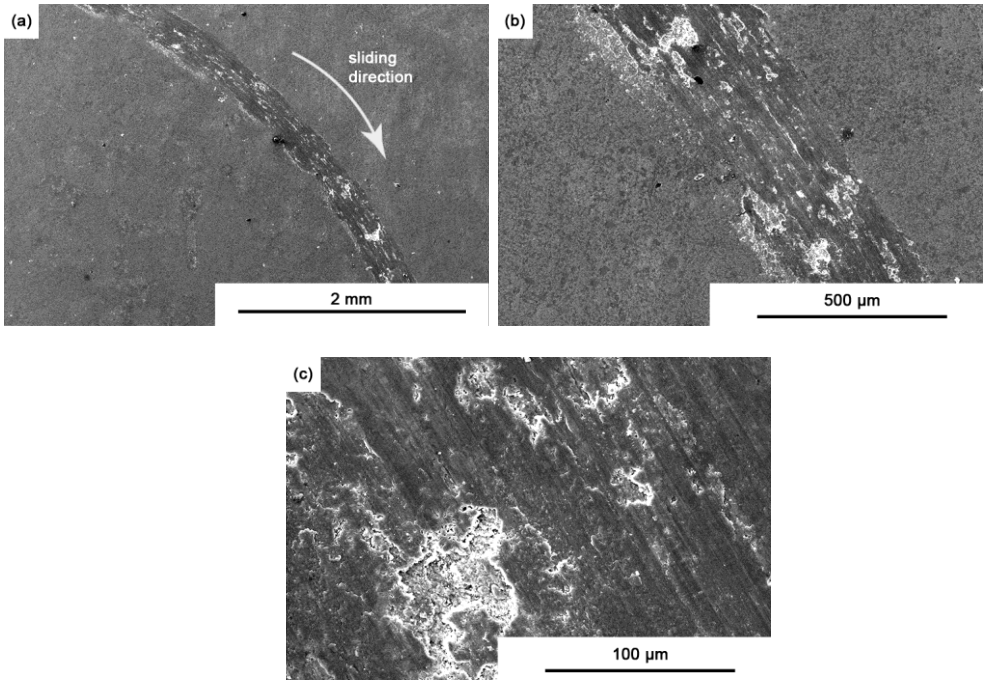

Figure 13. SEM micrographs of worn surfaces of Al-10% vol. MoS_2 composite sintered at 650 °C; (**a**–**c**) show different magnification of the same spot.

The lower friction coefficient, combined with the change in wear characteristics, allows for a significant reduction in material wear during testing—about 30 times—ranging from a wear coefficient value of 6.54×10^{-3} mm^3/Nm for the material sintered at 550 °C to approximately 0.27×10^{-3} mm^3/Nm for the materials sintered at 650 °C. (Figure 14). The surface topography and wear profiles are presented in Figures 15 and 16.

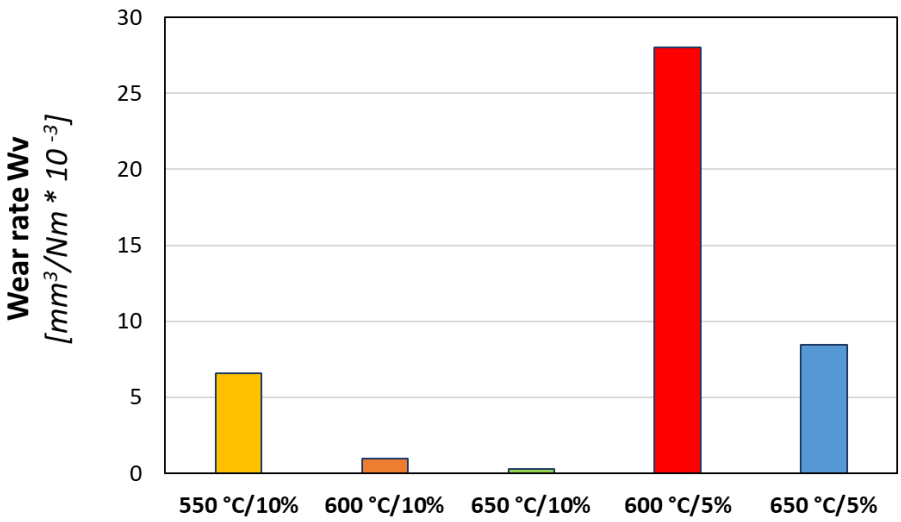

Figure 14. Material consumption rates during the ball-on-disc test of Al/MoS_2 composites.

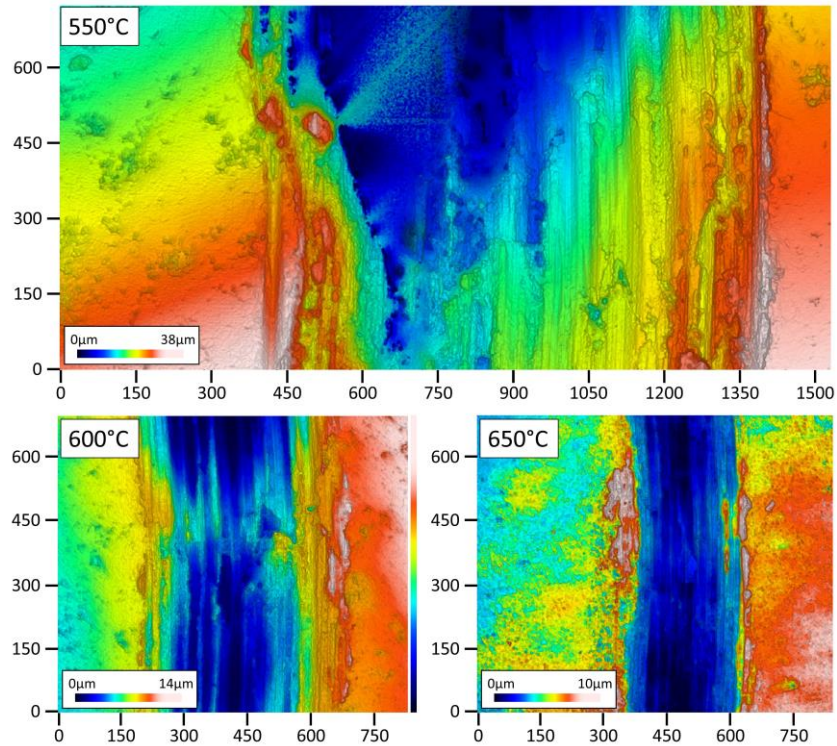

Figure 15. Surface topography of the wear traces from the ball-on-disc method of Al-10% vol. MoS_2 composites sintered at various temperatures.

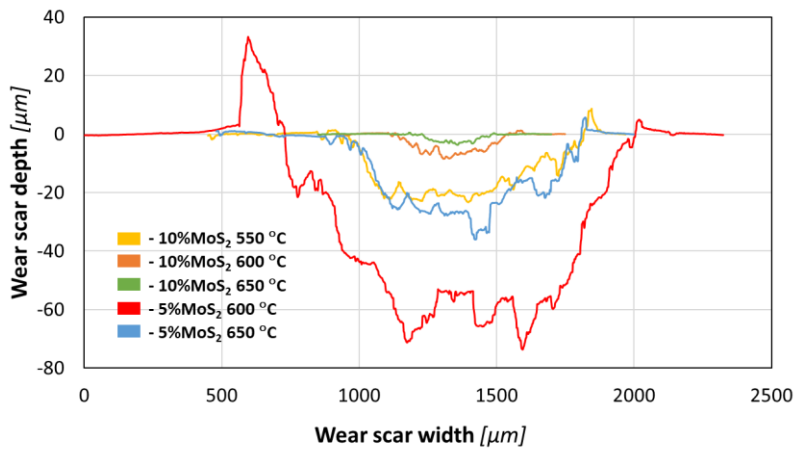

Figure 16. Wear track cross-section profiles after ball-on-disc tests of Al-10% vol. MoS_2 composites.

In the case of materials with the addition of 5% MoS_2, the initial values of the friction coefficient are much higher compared to those of materials with the addition of 10% MoS_2 (approx. 0.8 for 5% MoS_2 and 0.4 for 10% MoS_2, respectively), and they increase rapidly in the initial phase of the test (Figure 9). Unlike the materials with the addition of 10% MoS_2, significant fluctuations in the friction coefficients occur during the test. In the case of both samples sintered at 600 °C and 650 °C, significant plastic deformation of the substrate is observed (Figures 17 and 18). This is the result of the increase in interactions between the counter-sample and the metallic substrate due to the decrease in the share of MoS_2, which does not sufficiently separate the friction pair. The increase in friction forces enables the plastic deformation of even a harder substrate (for material sintered at 650 °C), leading to the accumulation of worn material in the area of the abrasion trace and its sudden removal every certain number of revolutions, which results in an increase in the friction coefficient. The change in the mechanism of interaction of the sample and counter-sample translates

into a significant increase in wear rates compared to materials with 10% MoS_2 from approx. 0.99×10^{-3} to 28×10^{-3} mm^3/Nm for sinters produced at 600 °C, and from 0.27×10^{-3} to approx. 8.47×10^{-3} mm^3/Nm for sinters produced at 650 °C (Figure 14).

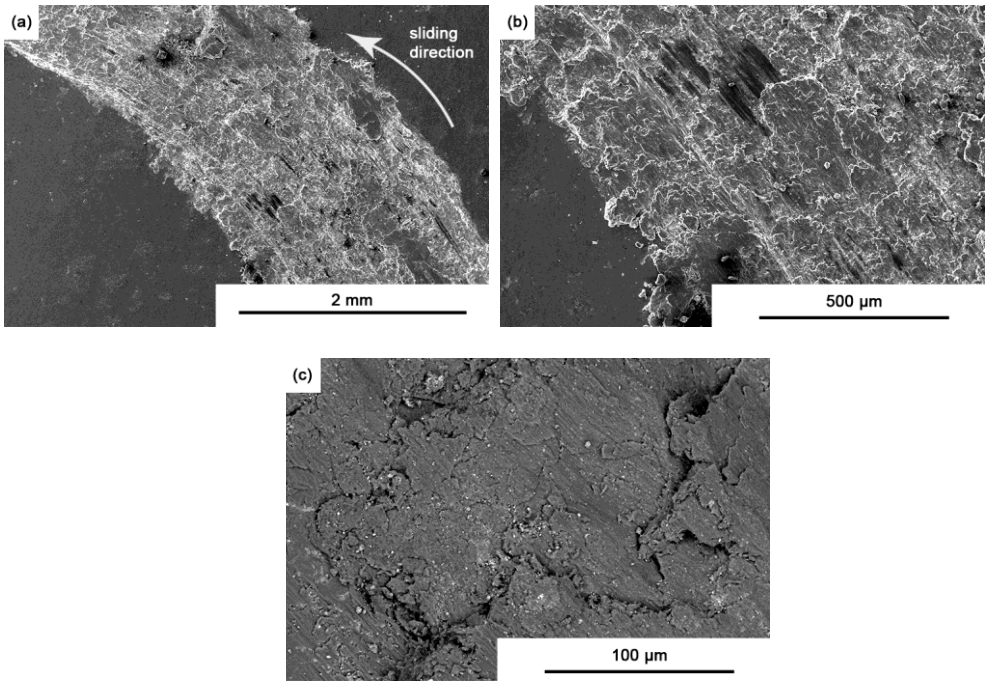

Figure 17. SEM micrographs of the worn surfaces of Al-5% vol. MoS_2 composite, sintered at 600 °C; (**a**–**c**) show different magnification of the same spot.

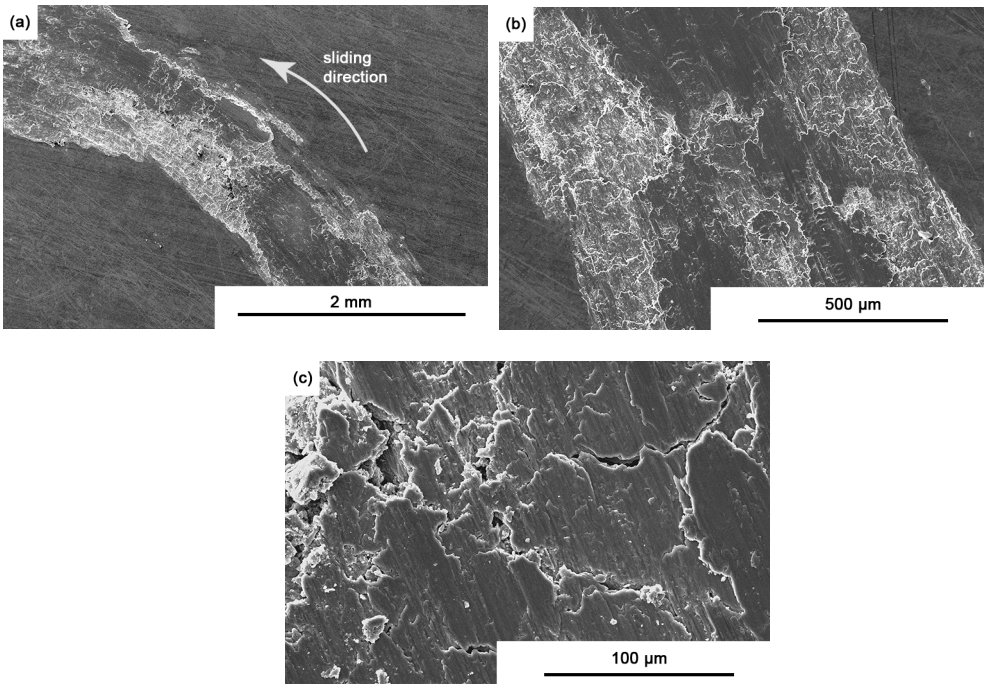

Figure 18. SEM micrographs of worn surfaces of Al-5% vol. MoS_2 composite, sintered at 650 °C; (**a**–**c**) show different magnification of the same spot.

4. Conclusions

The proposed SPS sintering process of pure aluminum-based composites with MoS_2 nanoflakes (5% and 10% by volume) leads to obtaining a coherent material with improved mechanical properties. As a result of the sintering process, a reaction occurs between the components of the composites, and a significant number of intermetallic phases are produced. Stereological analysis of selected micro-areas indicates that at the highest sintering temperature used, the total number of phases produced exceeds 50% by volume. At the same time, a certain amount of molybdenum sulfide remains in the structure, which constitutes a solid lubricant, enabling the improvement of the tribological properties.

It was confirmed that the amount of intermetallic phase generated in situ is strongly dependent on process parameters such as temperature and sintering time. The best degree of densification and the highest proportion of precipitates were obtained at the highest sintering temperature of 650 °C, which is related to the melting point of pure aluminum. The highly effective reaction of the ingredients results from intensive diffusion processes at a temperature close to the melting point. For composites with 5% content, significant participation of the liquid phase in the process was confirmed at a sintering time of t = 16 min, which was not observed for composites with the addition of 10% MoS_2. This means that the optimal sintering time and temperature depend on the MoS_2 proportion. Taking into account the specificity of SPS processes, the presence of a liquid phase in micro-areas cannot be ruled out during shorter processes at lower temperatures.

The Vickers hardness of all the obtained composites increased compared to that of pure aluminum (24 HV). An increase in hardness was observed regardless of the parameters used. However, for the composites sintered at 650 °C, a sudden increase was observed. This can be related to the presence of intermetallic precipitates with reduced porosity as well as a reduction in the size of the obtained precipitates at the highest sintering temperature used. The addition of 5% and 10% MoS_2 with optimal process parameters increased the hardness of the composite compared to pure aluminum by six and over seven times, respectively.

The presence of hard precipitates of intermetallic phases $Al_{12}Mo$ and Al_5Mo completely changes the wear mechanism in the friction process. Composites produced at the lowest temperature do not show the possibility of forming a film on the friction surface, and the wear mechanism is mainly adhesive and results from the strong plastic deformation of the matrix material. Only the presence of hard particles of intermetallic phases translates into a higher level of yield stress and enables the delamination of MoS_2 flakes and the formation of a tribofilm that reduces the value of the friction coefficient. In the case of composites with a lower proportion of solid lubricant (5% MoS_2), despite the increase in hardness, the remaining lubricant particles are insufficient to create a lasting tribofilm, and the increase in friction forces contributes to a significant increase in wear compared to composites containing 10% of the additive. The full utility potential of the obtained materials should be revealed and can only be confirmed by tests carried out in a vacuum.

Author Contributions: Conceptualization, M.K.; methodology, M.K. and K.K.; formal analysis, M.K. and K.K.; investigation, M.K., D.M. and K.K.; data curation, M.K., D.M. and K.K.; writing—original draft preparation, M.K.; writing—review and editing, K.K. and A.R.O.; visualization, M.K. and K.K.; supervision, M.K. and A.R.O.; project administration, A.R.O.; funding acquisition, A.R.O. All authors have read and agreed to the published version of the manuscript.

Funding: This work was financially supported by the Faculty of Materials Science and Engineering at the Warsaw University of Technology as part of a statutory grant.

Data Availability Statement: The original contributions presented in the study are included in the article, further inquiries can be directed to the corresponding author.

Conflicts of Interest: The authors declare no conflicts of interest.

References

1. Dursun, T.; Soutis, C. Recent developments in advanced aircraft aluminium alloys. *Mater. Des.* **2014**, *56*, 862–871. [CrossRef]
2. Prasad, S.V.; Asthana, R. Aluminum metal–matrix composites for automotive applications: Tribological considerations. *Tribol. Lett.* **2004**, *17*, 445–453. [CrossRef]
3. Srinivasan, V.; Kunjiappan, S.; Palanisamy, P.A. Brief review of carbon nanotube reinforced metal matrix composites for aerospace and defense applications. *Int. Nano Lett.* **2021**, *11*, 321–345. [CrossRef]
4. Bhadauria, A.; Singh, L.K.; Laha, T. Effect of physio-chemically functionalized graphene nanoplatelet reinforcement on tensile properties of aluminum nanocomposite synthesized via spark plasma sintering. *J. Alloys Compd.* **2018**, *748*, 783–793. [CrossRef]
5. Bisht, A.; Kumar, V.; Li, L.H.; Chen, Y.; Agarwal, A.; Lahiri, D. Effect of warm rolling and annealing on the mechanical properties of aluminum composite reinforced with boron nitride nanotubes. *Mater. Sci. Eng. A* **2018**, *710*, 366–373. [CrossRef]
6. Hu, Z.; Chen, F.; Xu, J.; Nian, Q.; Lin, D.; Chen, C.; Zhu, X.; Chen, Y.; Zhang, M. 3D printing graphene-aluminum nanocomposites. *J. Alloys Compd.* **2018**, *746*, 269–276. [CrossRef]
7. Chawla, K.K. *Metal Matrix Composites: Composite Materials Science and Engineering*; Springer: New York, NY, USA, 2012.
8. Daniel, B.S.S.; Murthy, V.S.R. Directed melt oxidation and nitridation of aluminium alloys: A comparison. *Mater. Des.* **1995**, *16*, 155–161. [CrossRef]
9. Pramod, S.L.; Bakshi, S.R.; Murty, B.S. Aluminum-Based Cast in Situ Composites: A Review. *J. Mater. Eng. Perform.* **2015**, *24*, 2185–2207. [CrossRef]
10. Matsunage, M.; Hoshimoto, K.; Uchiyama, Y. Frictional behaviour of molybdenum disulphide in high vacuum. *Wear* **1972**, *22*, 185–192. [CrossRef]
11. Arnell, R.D.; Davies, P.B.; Halling, J.; Whomes, T.L. *Tribology—Principles and Design Applications*; Macmillan: London, UK, 1991.
12. Kato, H.; Takama, M.; Iwai, Y.; Washida, K.; Sasaki, Y. Wear and mechanical properties of sintered copper–tin composites containing graphite or molybdenum disulfide. *Wear* **2003**, *255*, 573–578. [CrossRef]
13. Xiao, J.K.; Zhang, W.; Liu, L.M.; Zhang, L.; Zhang, C. Tribological behavior of copper-molybdenum disulfide composites. *Wear* **2017**, *384*, 61–71. [CrossRef]
14. Furlan, K.P.; Prates, P.B.; Santos, T.A.; Gouvêa Dias, M.V.; Ferreira, H.T.; Rodrigues Neto, J.B.; Klein, A.N. Influence of alloying elements on the sintering thermodynamics, microstructure and properties of Fe–MoS_2 composites. *J. Alloys Compd.* **2015**, *652*, 450–458. [CrossRef]
15. Joseph, J.S.D.; Kumaragurubaran, B.; Sathish, S. Effect of MoS_2 on the Wear Behavior of Aluminium (AlMg0.5Si) Composite. *Silicon* **2020**, *12*, 1481–1489. [CrossRef]
16. Kumaar, R.K.; Vinoth, K.S.; Kavitha, M. Dry sliding wear performance of AA7075/MoS_2 composite materials. *J. Eng. Res.* **2022**, *10*, 235–245. [CrossRef]
17. Bai, J.; Song, J.; Wei, J. Tribological and mechanical properties of MoS_2 enhanced polyamide 12 for Selective Laser Sintering. *J. Mater. Process. Technol.* **2019**, *264*, 382–388. [CrossRef]
18. Peng, H.; Wang, D.; Fu, S. Tannic acid-assisted green exfoliation and functionalization of MoS_2 nanosheets: Significantly improve the mechanical and flame-retardant properties of polyacrylonitrile composite fibers. *Chem. Eng. J.* **2020**, *384*, 123288. [CrossRef]
19. Kumar, V.; Gautam, R.K.; Tyagi, R. Tribological behavior of Al-based self-lubricating composites. *Compos. Interfaces* **2016**, *23*, 481–492. [CrossRef]
20. Daniel, A.A.; Murugesan, S.; Manojkumar, S.S. Dry Sliding Wear Behaviour of Aluminium 5059/SiC/MoS_2 Hybrid Metal Matrix Composites. *Mater. Res.* **2017**, *20*, 1697–1706. [CrossRef]
21. Liu, S.; Wang, Y.; Muthuramalingam, T.; Anbuchezhiyan, G. Effect of B_4C and MoS_2 reinforcement on micro structure and wear properties of aluminum hybrid composite for automotive applications. *Compos. B Eng.* **2019**, *176*, 107329. [CrossRef]
22. Ul Haq, M.I.; Raina, A.; Anand, A.; Sharma, S.M.; Kumar, R. Elucidating the Effect of MoS_2 on the Mechanical and Tribological Behavior of AA7075/Si_3N_4 Composite. *J. Mater. Eng. Perform.* **2020**, *29*, 7445–7455. [CrossRef]
23. Rajesh, S.; Velmurugan, C. Investigation of Wear Behaviour of Al6061 reinforcement with TiC and MoS_2. *J. Adv. Chem.* **2017**, *13*, 32–34. [CrossRef]
24. Vuddagiria, H.K.; Ravisankar, H. Estimation of Wear Performance of Al-based Composite Reinforced with Al_2O_3 and MoS_2 Using Taguchi Approach. *Tribol. Ind.* **2022**, *4*, 24–38. [CrossRef]
25. Rouhi, M.; Moazami-Goudarzi, M.; Ardestani, M. Comparison of effect of SiC and MoS_2 on wear behavior of Al matrix composites. *Trans. Nonferrous Met. Soc. China* **2019**, *29*, 1169–1183. [CrossRef]
26. Kanthavel, K.; Sumesh, K.R.; Saravanakumar, P. Study of tribological properties on Al/Al_2O_3/MoS_2 hybrid composite processed by powder metallurgy. *Alex. Eng. J.* **2016**, *55*, 13–17. [CrossRef]
27. Wozniak, J.; Kostecki, M.; Cygan, T.; Buczek, M.; Olszyna, A. Self-lubricating aluminium matrix composites reinforced with 2D crystals. *Compos. B Eng.* **2017**, *111*, 1–9. [CrossRef]
28. Kostecki, M.; Petrus, M.; Woźniak, J.; Cygan, T.; Olszyna, A. Closed Die Upsetting of Aluminum Matrix Composites Reinforced with Molybdenum Disulfide Nanocrystals and Multilayer Graphene, Implemented using the SPS Process—Microstructure Evolution. *Materials* **2018**, *11*, 994. [CrossRef]
29. Fan, L.; Yang, L.; Zhao, D.; Ma, L.; He, C.; He, F.; Shi, C.; Sha, J.; Zhao, N. Balancing Strength and Ductility in Al Matrix Composites Reinforced by Few-Layered MoS_2 through In-Situ Formation of Interfacial $Al_{12}Mo$. *Materials* **2021**, *14*, 3561. [CrossRef]

30. Ujah, C.O.; Aigbodion, V.S.; Ezema, I.I.C.; Makhatha, M.E. Spark plasma sintering of aluminium composites—A review. *Int. J. Adv. Manuf. Technol.* **2021**, *112*, 1819–1839. [CrossRef]
31. Saunders, N. The Al-Mo (aluminum-molybdenum) system. *J. Phase Equilibria* **1997**, *18*, 370–378. [CrossRef]
32. Lei, L.; Wang, L.; Wang, X. Reaction Mechanism and Synthesis of Ni_3Al–MoS_2 Matrix Self-Lubricating Composites Using Ni, Al, and MoS_2 Powders. *J. Inorg. Organomet. Polym. Mater.* **2018**, *28*, 223–234. [CrossRef]
33. Wiberg, E.; Wiberg, N.; Holleman, A.F. *Inorganic Chemistry*; Academic Press: San Diego, CA, USA; De Gruyter: Berlin, Germany, 2001.
34. Ozisik, H.; Deligoz, E.; Colakoglu, K.; Ozisik, H.B. Density functional study of the mechanical and phonon properties of $Al_{12}X$ (X = Mo, Tc, Ru, W, Re, and Os) compounds. *Intermetallics* **2014**, *50*, 1–7. [CrossRef]

Disclaimer/Publisher's Note: The statements, opinions and data contained in all publications are solely those of the individual author(s) and contributor(s) and not of MDPI and/or the editor(s). MDPI and/or the editor(s) disclaim responsibility for any injury to people or property resulting from any ideas, methods, instructions or products referred to in the content.